LAWRENCE
LIVERMORE
NATIONAL
LABORATORY

LLNL-CONF-636436

Multi-Fluid Geothermal Energy Production and Storage in Stratigraphic Reservoirs

T. A. Buscheck, M. Chen, Y. Hao, J. M. Bielicki, J. B. Randolph, Y. Sun, H. Choi

May 13, 2013

2013 Geothermal Resources Council Annual Meeting
Las Vegas, NV, United States
September 29, 2013 through October 2, 2013

Disclaimer

This document was prepared as an account of work sponsored by an agency of the United States government. Neither the United States government nor Lawrence Livermore National Security, LLC, nor any of their employees makes any warranty, expressed or implied, or assumes any legal liability or responsibility for the accuracy, completeness, or usefulness of any information, apparatus, product, or process disclosed, or represents that its use would not infringe privately owned rights. Reference herein to any specific commercial product, process, or service by trade name, trademark, manufacturer, or otherwise does not necessarily constitute or imply its endorsement, recommendation, or favoring by the United States government or Lawrence Livermore National Security, LLC. The views and opinions of authors expressed herein do not necessarily state or reflect those of the United States government or Lawrence Livermore National Security, LLC, and shall not be used for advertising or product endorsement purposes.

Multi-Fluid Geothermal Energy Production and Storage in Stratigraphic Reservoirs

Thomas A. Buscheck[a], Mingjie Chen[a], Yue Hao[a], Jeffrey M. Bielicki[b], Jimmy B. Randolph[c], Yunwei Sun[a], and Hyungjin Choi[c]

[a]Lawrence Livermore National Laboratory (LLNL)
P.O. Box 808, L-223, Livermore, CA 94550, USA, email: buscheck1@llnl.gov
[b]The Ohio State University, Columbus, OH, USA
[c]University of Minnesota, Minneapolis, MN USA

Key Words: geothermal energy, energy storage, sedimentary formations, artesian flow, reservoir simulation

Abstract

Stratigraphic reservoirs (in sedimentary formations) are an under-explored play concept because they are typically associated with a conductive thermal regime, requiring greater depths to reach economic temperatures than hydrothermal upflows. On the other hand, stratigraphic reservoirs offer the advantages of higher permeability (and transmissivity), extending over much larger areas (> 100 km^2) than typical upflows (< 3 km^2), and have lower, predictable drilling risk. These make an attractive target for geothermal development, but several challenges need to be addressed. The primary challenge is to maximize heat extraction, while minimizing drilling and extraction costs. To increase extraction efficiency, we propose injecting supplemental fluids (CO_2 and/or N_2) to augment reservoir pressure, thereby enhancing fluid production rates. Because N_2 can be readily separated from air, pressure augmentation can occur during periods of low grid power demand, which will reduce costs and enable energy storage. A well pattern consisting of a minimum of four concentric rings of horizontal producers and injectors is proposed to conserve pressure from injection operations, minimize loss of supplemental fluids, generate large artesian flow rates that take advantage of the large productivity of horizontal wells, and segregate the supplemental fluid and brine production zones. We present simulations of this approach for an idealized reservoir model, consisting of a relatively permeable sedimentary formation, vertically confined by two impermeable seal units. More realistic (heterogeneous) geologic settings and wellbore flow effects will be considered in future studies to more rigorously evaluate the potential economic advantages of this approach.

1. Introduction

Economic viability of geothermal energy production requires a resource with the necessary temperature to yield individual well heat extraction rates that are sufficient to justify project development costs. Geothermal energy production can be limited by insufficient working fluid and pressure depletion. This depletion increases the parasitic cost of powering the fluid recirculation system, which can include the expense of submersible pumps. Sedimentary basins are often associated with low resource temperatures; but, these resources have higher permeability (extending over much larger areas) than the geologic settings for conventional hydrothermal systems, with much of that advantage being matrix (rather than fracture) permeability. Because of their high permeability, these basins may be used for geologic CO_2 storage (GCS). The NATCARB Regional Carbon Sequestration Partnership (RCSP) database (Carr et al., 2007) has identified extensive regions suitable for GCS. A significant subset of this area has high enough temperature to be of economic value for CO_2-based geothermal energy production (Elliot et al., 2013).

Geothermal energy production and GCS can contribute to lowering atmospheric CO_2 emissions, necessary for mitigating climate change (IPPC, 2005; Socolow and Pacala, 2006). For large-scale GCS, overpressure can limit the ability to store CO_2, while geothermal energy production can be limited by pressure depletion (Buscheck et al., 2012a; 2012b; 2012c). It is possible to synergistically integrate these systems, with CO_2 injection providing pressure support to maintain the productivity of geothermal brine producers, while the net loss of brine provides pressure relief and improved injectivity for CO_2 injectors. A CO_2-based, enhanced geothermal energy system (EGS) concept, using CO_2 instead of water as the working fluid, was first proposed by Brown (2000). Pruess (2006) followed up on his idea by analyzing

reservoir behavior and found CO_2 to be superior to water in mining heat from hot fractured rock, including reduced parasitic power consumption to drive the fluid recirculation system. This concept has been extended to GCS in sedimentary formations (Randolph and Saar, 2011a; 2011b; 2011c; Saar et al., 2010), and deemed a CO_2-Plume Geothermal (CPG) system, to distinguish it from CO_2-enabled EGS in crystalline rock. Because it is targeted for large, porous, permeable sedimentary basins, CPG can result in more CO_2 sequestration and more heat extraction than CO_2-based EGS in crystalline rock.

2. Multi-Fluid, Multi-Ring, Horizontal-Well Approach

While most research on CO_2-based geothermal systems has emphasized using CO_2 as a working fluid (Pruess, 2006; Randolph and Saar, 2011a; 2011b, 2011c), it is possible to expand on this idea by using CO_2 as a pressure-support fluid to generate artesian pressures to drive brine production (Buscheck et al., 2013). To address the high cost of CO_2 captured from fossil-fueled power plants, and to provide operational flexibility, we further expand on this idea with the addition of N_2 as a supplemental working fluid. N_2 is advantageous because it can be separated from air at low cost, compared to CO_2, it is non-corrosive and will not react with the formation, and has no raw material supply risk. The addition of N_2 can improve the economics of brine- or brine-/CO_2-based geothermal energy production and mitigates possible operational issues associated with CO_2, such as flashing in the wellbore.

Our proposed multi-fluid geothermal energy production approach uses concentric rings of horizontal wells, with the option of multiple levels (Figure 1), to create a hydraulic divide to conserve supplemental working fluid and pressure, store energy, and drive brine to the outer producers. Similar to enhanced oil recovery (EOR) operations that inject CO_2, N_2, or air (Haley et al., 2002); our approach takes advantage of gravity-drainage, double-displacement to enhance the recovery of liquids. The addition of a supplemental fluid also generates excess make-up brine for heat extraction, reinjection, and power-plant cooling. Initially, only native brine is produced; however, as the supplemental fluids reach the producers, fluid recovery transitions from brine to N_2 and/or CO_2. Hence, this approach takes advantage of using multiple working fluids for heat extraction. A key goal is for brine production rates (per well) to exceed the capacity of submersible pumps to take advantage of the large productivity of long-reach horizontal wells. This enables greater leveraging of well costs, particularly valuable for deep geothermal resources. Production rates of CO_2 and N_2 can also be high, driven by the thermosiphon effect (Adams et al., 2013).

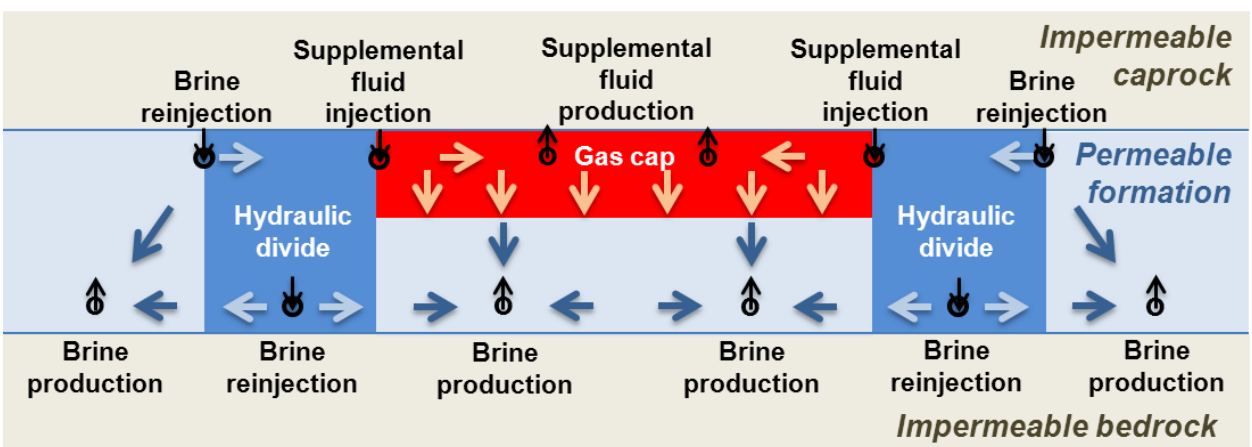

Figure 1. Schematic of multi-fluid, multi-ring, horizontal-well approach is shown.

For reasons discussed later, this approach requires a well pattern consisting of a minimum of four concentric rings of horizontal producers and injectors (Figure 2). The inner ring consists of brine/CO_2/N_2 producers and the second ring consists of CO_2/N_2 injectors. The third and fourth rings consist of brine reinjectors and producers, respectively. Each of these rings can include additional rings at different depths

(Figure 1) to provide better control of fluid and energy recovery for improved sweep efficiency, which would reduce thermal drawdown and increase project lifetime. This configuration can take advantage of the fact that horizontal-well drilling technology developed in the oil and gas industry allows for precise directional control; hence, it is realistic to create precisely curved injection and production intervals.

Using four concentric rings conserves pressure from injection operations and minimizes the loss of CO_2 and N_2. This configuration implements a novel hydraulic-divide strategy to assure that only the inner-ring producers will ever extract CO_2 and N_2 and that the outer-ring producers will only extract brine (Figure 2). The outer ring creates a hydraulic trough to limit the lateral extent of overpressure, as well as to capture any CO_2 and N_2 that may pass through the hydraulic divide. This configuration spreads overpressure to limit its magnitude and reduce the risks of induced seismicity and CO_2 leakage. An advantage of this approach is that storage of CO_2 and N_2 displaces (and frees up) an equivalent volume of formation brine for recirculation, as well as for power-plant cooling, which can be particularly valuable in arid regions where air-cooling may otherwise be necessary. Because brine comes from the same formation as that used for injection, it reduces the possibility of chemical incompatibility, which could be an issue if brine came from a separate formation.

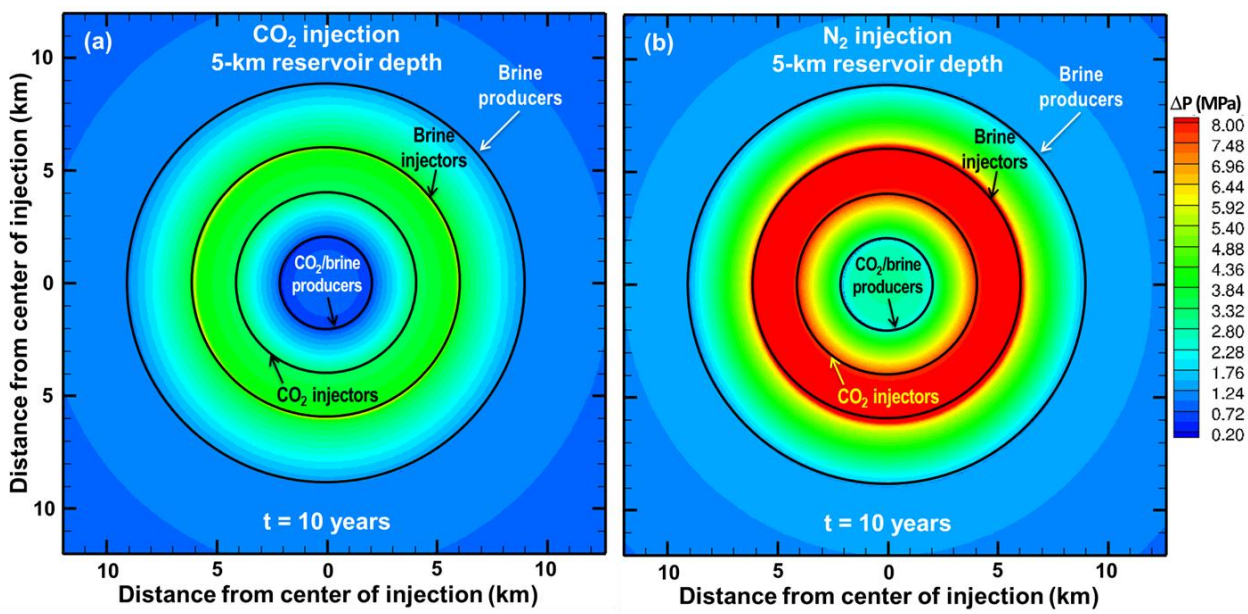

Figure 2. Overpressure ΔP at the elevation of injectors and producers for (a) CO_2 injection and (b) N_2 injection.

3. Modeling Approach

Reservoir analyses were conducted with the NUFT code, which simulates multi-phase heat and mass flow and reactive transport in porous media (Nitao, 1998). The pore and water compressibility are 4.5×10^{-10} and 3.5×10^{-10} Pa^{-1}, respectively. Water density is determined by the ASME steam tables (ASME, 2006). The two-phase flow of supercritical CO_2 and water was simulated with the density and compressibility of supercritical CO_2 determined by the correlation of Span and Wagner (1996) and viscosity determined by the correlation of Fenghour et al. (1997). The two-phase flow of supercritical N_2 and water was simulated with the density and compressibility for N_2 determined by correlation of Span et al. (2000) and the viscosity determined by the correlation of Lemmon and Jacobsen (2004).

A generic system is modeled, consisting of a 250-m-thick reservoir with a permeability of 1×10^{-13} m^2, bounded by impermeable (caprock and bedrock) seal units with a permeability of 1×10^{-18} m^2. Hydrologic properties (Table 1) are similar to previous GCS and GCS-geothermal studies (Zhou et al., 2008; Buscheck et al., 2012a; 2012b; 2012c; 2013). Because conditions are assumed to be laterally

homogeneous, we can use a radially-symmetric (RZ) model. A geothermal gradient of 37.5°C/km and a reservoir bottom depth of 5 km are considered. The RZ model is representative of rings of arc-shaped horizontal wells. Using an RZ model allows for fine mesh refinement, particularly around the injectors and producers to better model pressure gradients close to the wells. Gridblocks representing the injector and producer rings have dimensions similar to those of wellbores.

With respect to supplemental fluid injection, NUFT is used to model two cases: (1) pure supercritical CO_2 injection and (2) pure supercritical N_2 injection. We use the reservoir model results to determine brine-based, Organic Rankine Cycle binary-power generation, using the GETEM code (DOE, 2012). Geothermal energy is extracted from produced CO_2 and N_2 at the surface using a direct-cycle power system, in which the produced CO_2 and/or N_2 is itself sent through a turbine rather than a binary-power system. For CO_2 and N_2 working fluids, direct-power systems offer much greater energy conversion efficiency than binary systems because the supercritical fluids generate a substantial pressure difference between the hot production wellhead and the cold injection wellhead, while simultaneously losing considerable temperature during their rise in production wells. The latter effect – Joule-Thomson cooling – causes low binary-system efficiency compared to brine-based systems operating at similar reservoir temperatures. We assume that produced brine has been separated from the produced CO_2 and/or N_2 prior to sending those fluids through the turbine for power extraction. Because the energy penalty for fluid separation is minor, we have neglected it from our power-generation analyses.

Currently, the NUFT code cannot handle mixtures of CO_2 and N_2; however, we analyze power generation for cases with injected CO_2/N_2 mixtures, assuming that CO_2 and N_2 are perfectly mixed in the supercritical-fluid phase and fluid production and heat extraction histories are calculated as a linear interpolation. All produced CO_2 (or N_2) is reinjected into the second ring and all produced brine is reinjected into the third ring. Initially, CO_2 (or N_2) injection rate is 480 kg/sec (15.2 MT/year), which is gradually increased to keep pace with the increasing CO_2 (or N_2) production. As produced CO_2 (or N_2) begins to be recirculated, it is not necessary to deliver 15.2 MT/year to maintain the targeted injection rate. Thus, the option exists to reduce the delivery rate of captured CO_2 or separated N_2, unless it is desired to increase fluid production rates.

Table 1. Hydrologic property values used in the study are listed.

Property	Reservoir/Storage Formation	Caprock and bedrock seal units
Horizontal and vertical permeability (m^2)	1.0×10^{-13}	1.0×10^{-18}
Pore compressibility (Pa^{-1})	4.5×10^{-10}	4.5×10^{-10}
Porosity	0.12	0.12
van Genuchten (1980) *m*	0.46	0.46
van Genuchten α (Pa^{-1})	5.1×10^{-5}	5.1×10^{-5}
Residual supercritical CO_2 saturation	0.05	0.05
Residual water saturation	0.30	0.30

For the case of pure CO_2 or pure N_2 production, the power-system model simulates fluid flow through a direct-power system, heat rejection through a cooling apparatus, and pumping prior to reinjection, if required. The model accounts for frictional losses in surface equipment and piping (ε = 0.000055 m), as well. The isentropic efficiency for the power system and pumps are set at 90 and 80 percent, respectively (Adams et al., 2013). Power generation for cases involving a produced fluid mixture of CO_2 and N_2 are calculated as a linear interpolation, at constant production temperature/pressure and varying composition, of the pure fluid cases. Future analyses will directly simulate power production for mixed fluid cases. The power system model is optimized for net electricity generation, which may not be the economic optimum. We assume an average annual atmospheric temperature of 12°C, a turbine outlet temperature of 27°C, a turbine approach temperature of 15°C, and a cooling-system approach temperature of 10°C.

We model a four-ring pattern of horizontal wells (Figure 2) with all of the wells completed at the bottom of the reservoir, at a depth of 5 km (Figures 3 and 4). The inner production ring has a radius of 2 km. The second ring, representing CO_2 (or N_2) injectors, has a radius of 4 km. The third ring, representing brine injectors, has a radius of 6 km, and the fourth ring, representing brine producers, has a radius of 9 km. The bottom-hole pressure of the producers is fixed to be 1.0 MPa greater than the ambient reservoir pressure at a 5 km depth. This assumed bottom-hole pressure allows artesian flow up the well, while accounting for friction loss. Future reservoir analyses will include multi-phase wellbore models of brine and supercritical CO_2 and N_2.

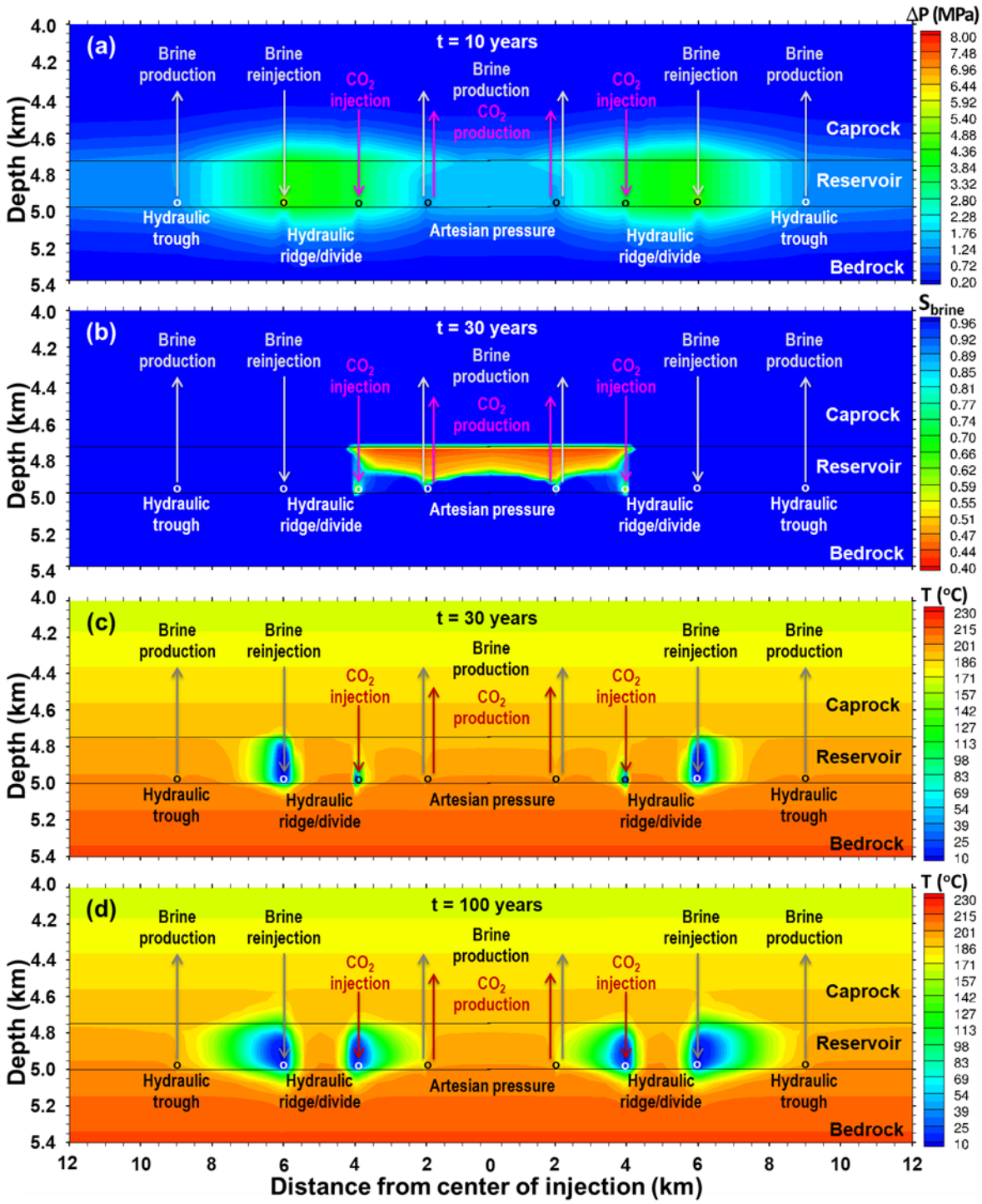

Figure 3. Four-ring horizontal-well pattern with CO_2 injection: (a) overpressure ΔP at 10 years, (b) brine saturation S_{brine} at 30 years, and (c,d) temperature T at 30 and 100 years.

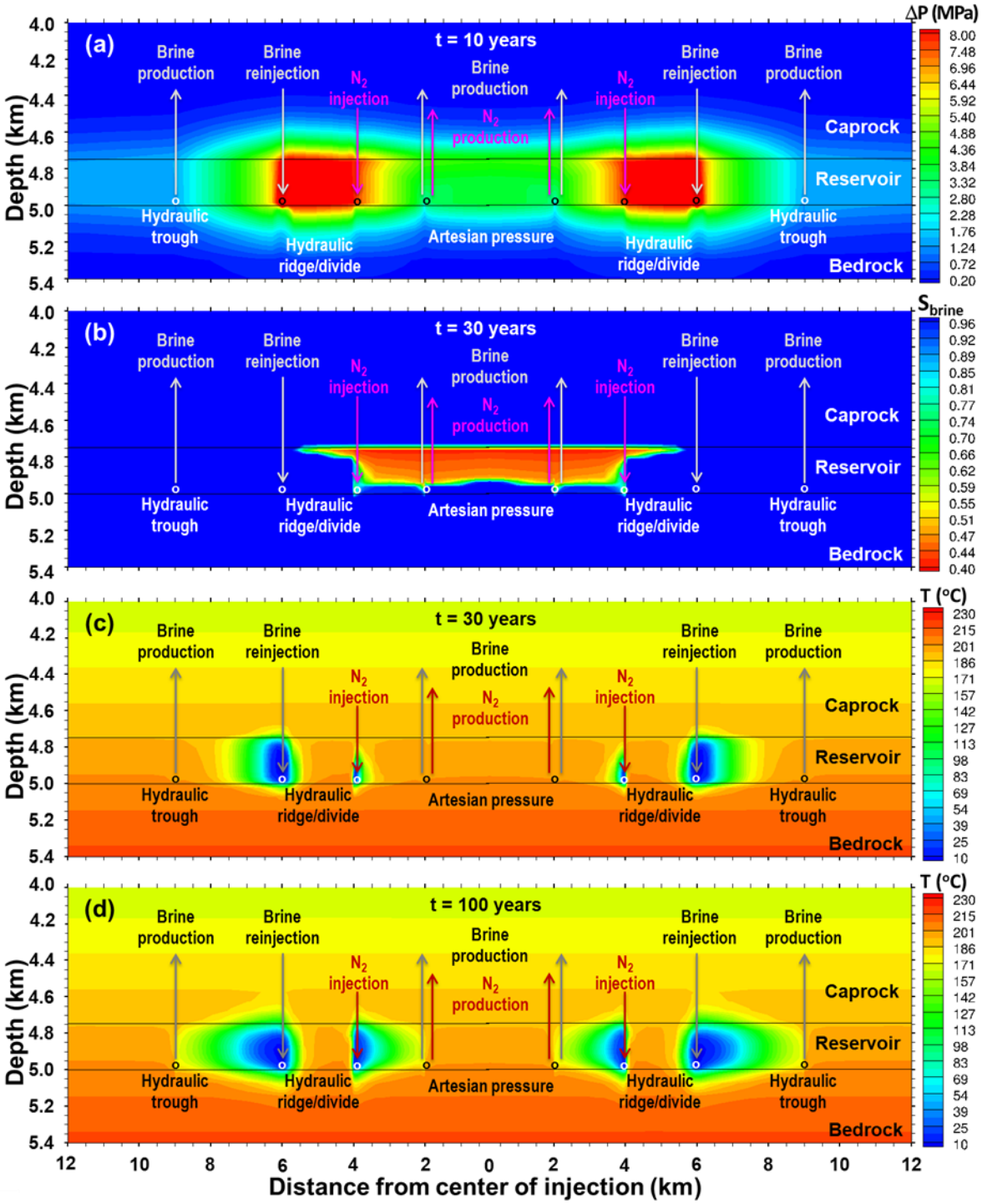

Figure 4. Four-ring horizontal-well pattern with N_2 injection: (a) overpressure ΔP at 10 years, (b) brine saturation S_{brine} at 30 years, and (c,d) temperature T at 30 and 100 years.

4. Results

We present reservoir analyses for the case where the supplemental fluid is supercritical CO_2 (Section 4.1) and for the case where it is supercritical N_2 (Section 4.2). Production histories (Figures 5 and 6) are compared for the CO_2- and N_2-injection cases for a 100 year injection/production period. In Section 4.3 we present the results for power generation from the respective working fluids.

4.1 Reservoir Analyses Brine/CO_2 Systems

We start with the case with supercritical CO_2 injection (Figures 2a, 3, 5, and 6). A zone of maximum overpressure develops between the second ring of CO_2 injectors and the third ring of brine reinjectors (Figures 2a and 3a). This creates a hydraulic divide that restricts lateral migration of CO_2 (Figure 3b), thereby limiting the loss of CO_2, while conserving overpressure from CO_2 injection. The hydraulic divide segregates the CO_2- and brine-driven thermal plumes (Figure 3c and d), causing CO_2 to only be produced at the inner ring; with the outer ring only producing brine (Figure 5a). Initially, the inner ring only produces brine (Figure 5a), which is reinjected in the third ring. Because brine reinjection occurs on the outer flank of the zone of overpressure (Figures 2a and 3a), it effectively drives flow "downhill" to the outer ring of producers, where it causes artesian flow. All brine produced in the outer ring is reinjected in the third ring, which helps maintain overpressure. Overpressure and inner-ring brine production continue to increase for 12 years (Figure 5a) whereupon CO_2 reaches the producers (Figure 5c). As CO_2 cut increases, inner-ring brine production decreases. Thus, there is less brine to be reinjected in the third ring, which reduces the outer-ring brine-production rate (Figure 5a). Note that the peak for outer-ring brine production lags slightly behind the peak for the inner producer ring. Cumulative brine production increases steadily, tapering off slightly at later time (Figure 6a). The mass ratio of cumulative brine production to net CO_2 storage is a measure of the "leveraging" benefit of CO_2 injection as a pressure-support fluid (Figure 6a); this ratio peaks at 30 years, with a value of 11.6, gradually decreasing to 9.6 at 100 years.

For the CO_2-injection case, peak overpressure never exceeds 5 MPa, which is ~10 percent of hydrostatic pressure for a depth of 5 km; which is far below fracture overpressure (typically approximated as 80 percent of hydrostatic pressure). Recall that a reservoir permeability of $1x10^{-13}$ m^2 was used; if we decreased that by a factor of 10 ($1x10^{-14}$ m^2), overpressure could exceed 80 percent of hydrostatic.

All produced CO_2 is reinjected in the second ring. Because one of our goals is to maximize the use of CO_2 as a working fluid, we continuously increased the CO_2 injection rate after CO_2 breakthrough (Figure 5a). Because it has a lower viscosity than brine, CO_2 is increasingly preferentially extracted at the inner production ring, allowing us to increase CO_2 injection from an initial rate of 480 kg/sec to 3800 kg/sec. As the region between the first and second rings fills with CO_2, flow resistance between these rings is reduced, due to the low CO_2 viscosity, allowing us to increase the CO_2 injection rate without increasing overpressure. As CO_2 cut increases, a greater fraction of produced CO_2 is recirculated CO_2, causing the ratio of cumulative CO_2 production to net CO_2 storage to gradually increase to a value of 6.8 at 100 years (Figure 6c). At 20 years, 54 percent of produced CO_2 is recirculated CO_2, while 81, 89, and 91 percent of CO_2 production is recirculated CO_2 at 30, 50, and 100 years, respectively (Figure 6e). The CO_2 delivery rate, which is the difference between injection and production rates, declines from 15.2 MT/year to 12.4 MT/year (Figure 6g).

Thermal mixing causes an immediate small decline in extraction temperature (Figure 5c), as cooler brine from the upper reservoir is drawn down to the producers at the bottom of the reservoir. CO_2 breakthrough causes a small decline in extraction temperature at 12 years for the inner ring (Figure 5c). Because of the low heat capacity of CO_2, compared to brine, thermal drawdown is minimal until ~75 years. Because of the greater (3-km) spacing between the third and fourth (outer) rings, and because production rate per unit length of producer is less for the outer producer ring than it is for the inner producer ring, thermal drawdown is much less for the outer ring than it is for the inner ring.

At 30 years, the thermal plumes have not reached either the inner or outer producers (Figure 3c). At 100 years, the inner thermal plume has reached the inner producers, while the outer thermal plume has not yet reached the outer producers (Figure 3d). Because of the negligible thermal decline for brine production, the brine-based heat extraction rate (Figure 5e) tracks exactly with the brine production rate (Figure 5a) for both the inner and outer producers. The CO_2-based heat extraction rate (Figure 5e) exactly follows the same trend as the CO_2 production rate (Figure 5a) until the thermal decline begins at ~75 years.

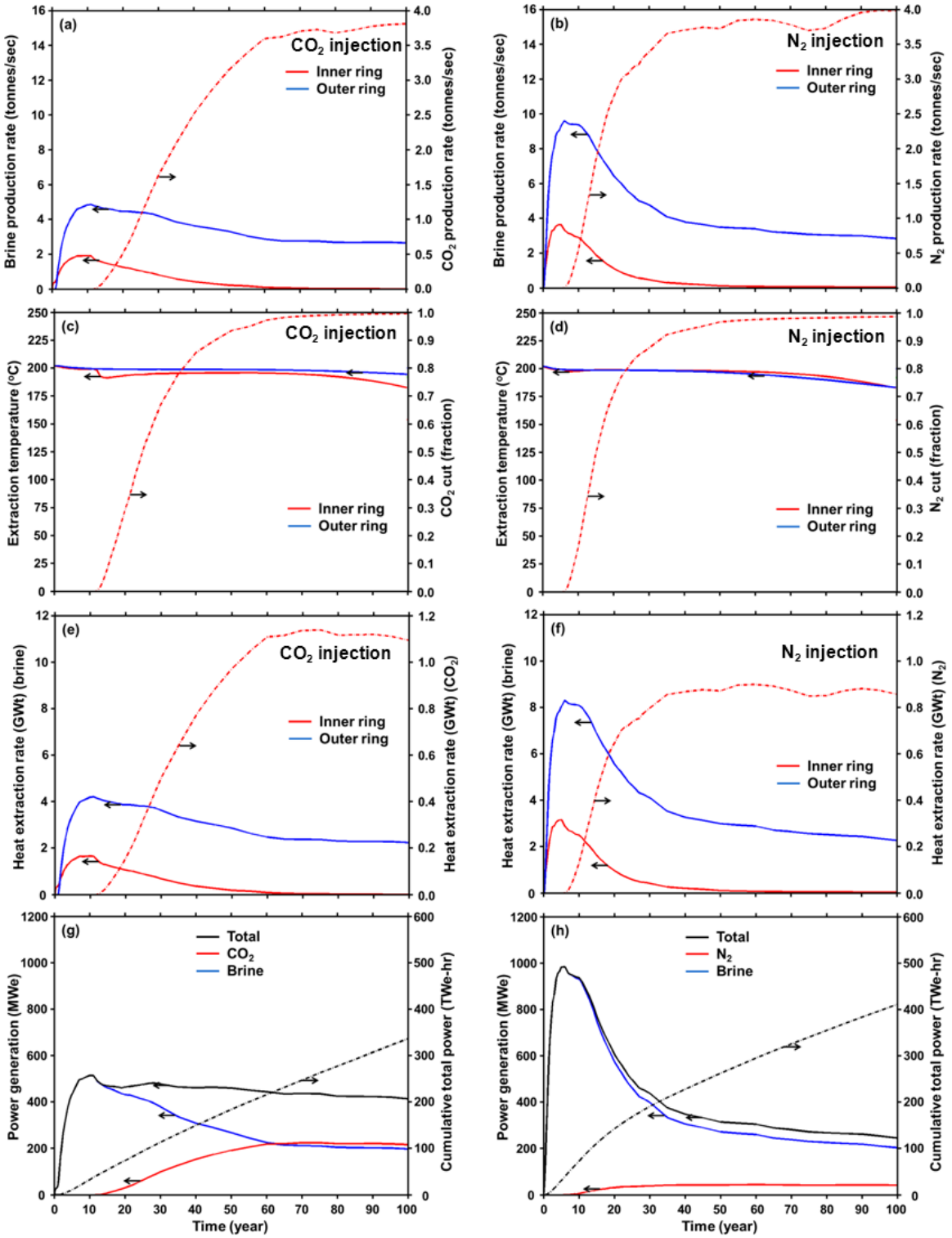

Figure 5. Four-ring horizontal-well pattern with (a,c,e,g) CO_2 injection and (b,d,f,h) N_2 injection: (a) brine and CO_2 production rate, (b) brine and N_2 production rate, (c,d) extraction temperature, (e) brine- and CO_2-based heat extraction rate, (f) brine- and N_2-based heat extraction rate, (g) brine- and CO_2-based electrical power generation, and (h) brine- and N_2-based electrical power generation.

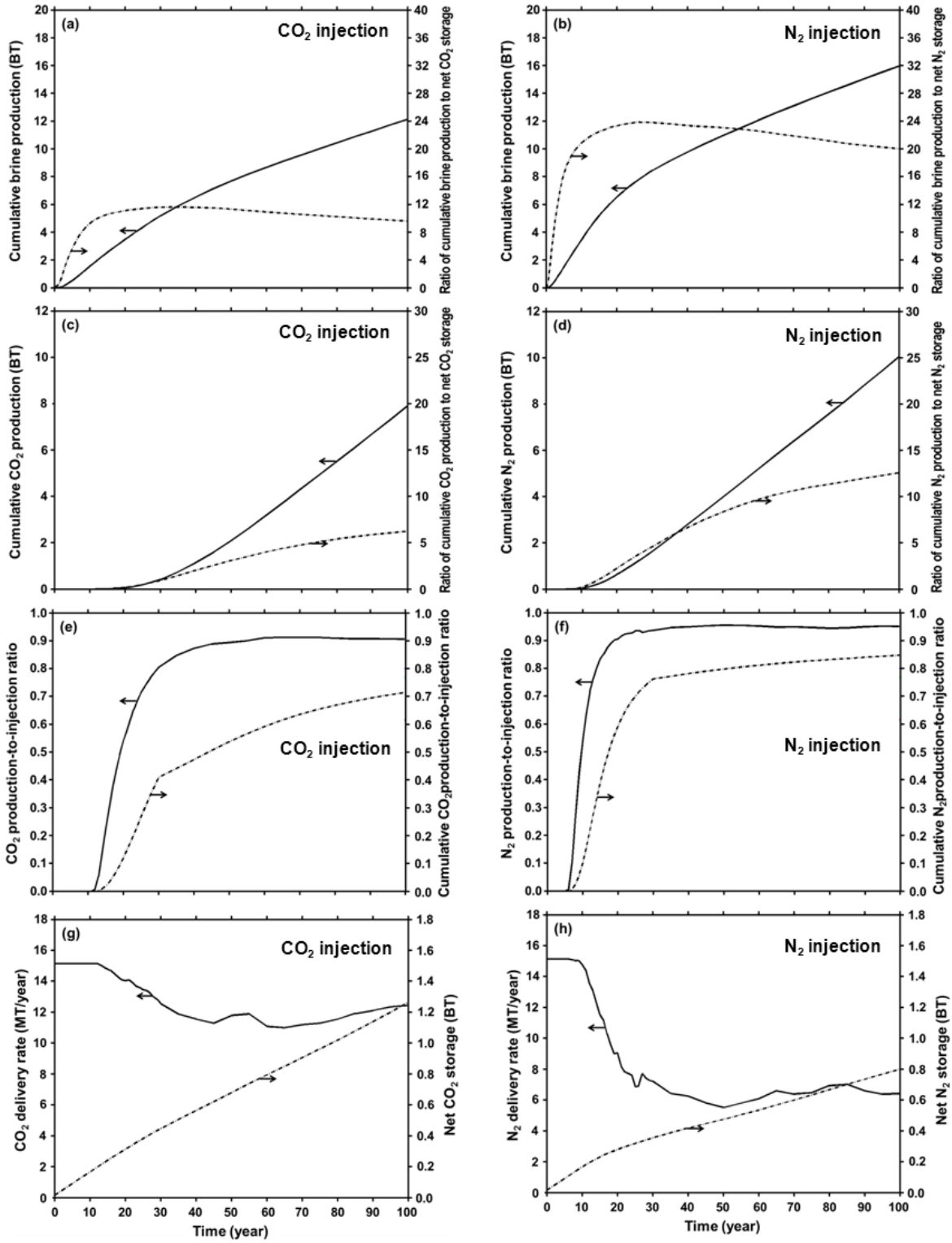

Figure 6. Four-ring horizontal-well pattern with (a,c,e,g) CO_2 injection and (b,d,f,h) N_2 injection: (a) cumulative brine production and ratio of cumulative brine production to CO_2 storage, (b) cumulative brine production and ratio of cumulative brine production to CO_2 storage, (c) cumulative CO_2 production and ratio of cumulative CO_2 production to CO_2 storage, (d) cumulative N_2 production and ratio of cumulative N_2 production to N_2 storage, (e) ratio of instantaneous CO_2 production to CO_2 injection and ratio of cumulative CO_2 production to CO_2 storage, (f) ratio of instantaneous N_2 production to N_2 injection and ratio of cumulative N_2 production to N_2 storage, (g) CO_2 delivery rate and net CO_2 storage, and (h) N_2 delivery rate and net N_2 storage.

4.2 Reservoir Analyses Brine/N_2 Systems

We now consider the case with supercritical N_2 injection (Figures 2b, 4, 5, and 6). As with CO_2-injection, a zone of maximum overpressure develops between the second ring of N_2 injectors and the third ring of brine reinjectors (Figures 2b and 4a). While the pattern of overpressure is qualitatively similar to that in the CO_2-injection case, N_2 injection creates twice the overpressure caused by CO_2 injection, due to its density being less than half that of CO_2 at reservoir temperature and pressure conditions. Accordingly, increasing overpressure by a factor of two nearly doubles the early-time brine production rates for both the inner and outer producers (compare Figure 5b with Figure 5a). Because N_2 viscosity is less than that of CO_2, and because of its lower density (and greater volume), N_2 reaches the inner ring of producers in just 6 years (half the time required for CO_2 breakthrough). The greater volume of the N_2 plume, compared to the CO_2 plume, continues to be apparent at 30 years (compare Figure 4b with Figure 3b). As with the CO_2-injection case, the hydraulic divide (Figure 4a) restricts the lateral migration of N_2 (Figure 4b).

Cumulative brine production increases very strongly at early time, with the rate of increase tapering off at later time (Figure 6b). The ratio of cumulative brine production to net N_2 storage peaks at 25 years, attaining a value of 24, gradually decreasing to 20 at 100 years. For the N_2-injection case this ratio is always at least twice that of the CO_2-injection case (Figures 6a and b). Therefore, on a per mass basis, N_2 is twice as effective as CO_2 as a pressure-support fluid for driving artesian brine production.

For the N_2-injection case, peak overpressure never exceeds 8 MPa, which is ~16 percent of hydrostatic pressure for a depth of 5 km; which is far below fracture overpressure. Overpressure and inner-ring brine production continue to increase for 6 years (Figure 5b) whereupon N_2 reaches the producers (Figure 5d). As N_2 cut increases, inner-ring brine production decreases. Consequently, there is less brine to be reinjected in the third ring, which reduces the outer-ring brine-production rate (Figure 5b). As in the CO_2-injection case, the peak in outer-ring brine production lags slightly behind the peak for the inner producer ring.

All produced N_2 is reinjected in the second ring. Because N_2 is increasingly preferentially extracted at the inner production ring, we could increase N_2 injection from an initial rate of 480 kg/sec to 4000 kg/sec. As the region between the first and second rings fills with low-viscosity N_2, flow resistance between these rings is reduced, allowing us to increase the N_2 injection rate without increasing overpressure. As N_2 cut increases, a greater fraction of produced N_2 is recirculated N_2, causing the ratio of cumulative N_2 production to net N_2 storage to gradually increase to a value of 12.6 at 100 years (Figure 6d), twice that of the CO_2-injection case (Figure 6c). Cumulative N_2 production is 10 BT (Figure 6d), greater than the value (7.9 BT) in the CO_2-injection case (Figure 6c). At 20 years, 91 percent of produced N_2 is recirculated N_2, while 94, 96, and 95 percent of N_2 production is recirculated N_2 at 30, 50, and 100 years, respectively (Figure 6f). The N_2 delivery rate, which is the difference between injection and production rates, declines from 15.2 MT/year to ~5 to ~7 MT/year (Figure 6h), roughly half that of the CO_2-injection case. The net storage of N_2 is 0.80 BT (Figure 6h), compared to 1.26 BT of net CO_2 storage in the CO_2-injection case (Figure 6g).

Thermal mixing causes an immediate small decline in extraction temperature (Figure 5d), as cooler brine from the upper reservoir is drawn down to the producers at the bottom of the reservoir. Because of the low heat capacity of N_2, compared to brine and CO_2, thermal drawdown is negligible at the inner production ring. The larger brine production rates causes the thermal plume to migrate faster in the N_2-injection case than in the CO_2-injection case (compare Figures 4c and d with Figures 3c and d). Thus, thermal drawdown begins earlier (~60 years) in the N_2-injection case than in the CO_2-injection case (compare Figure 5d with Figure 5c).

4.3 Power Generation for Brine/CO_2, Brine/N_2, and Brine/CO_2/N_2 Systems

Using GETEM (DOE, 2012), we built a brine-based, binary-cycle, net-power generation table for resource temperatures of 175, 200, and 225°C, and a depth of 5 km, assuming submersible pumps are not required. This table was used to create conversion efficiencies to convert from heat extraction rate to net-

power generation, which were used to interpolate values of conversion efficiency corresponding to the simulated extraction temperatures (Figure 5g and h). For CO_2-based and N_2-based, direct-turbine, power generation, we determined net power output, including all parasitic losses in the entire power system, including pumps and cooling equipment (Table 2). After applying the brine and CO_2 conversion efficiencies to the respective heat extraction rates, we determine brine-based, CO_2-based, and total net power generation (Figure 5g and h). At early time, power is entirely generated from brine production for both CO_2 and N_2 injection. Starting at 12 years, CO_2-based power generation begins (Figure 5g). The contribution of CO_2-based power increases with time until it is slightly greater than brine-based power. Starting at 6 years, N_2-based power begins (Figure 5h); however, the higher parasitic pumping cost for N_2 results in lower net power generation for N_2 than for CO_2. Tables 3 and 4 summarize power generation for the first 30 and 100 years, respectively, including power sales, and power sales per MT of net CO_2 storage.

Table 2. Gross and net turbine power, including parasitic pumping power, is summarized for CO_2 and N_2.

Temperature (^oC)	Gas mixture (CO_2/N_2)	Net power (kW/kg/sec)	Gross turbine power (kW/kg/sec)	Pumping power (kW/kg/sec)	Efficiency (%)
200	100/0	46.5	57.3	5.1	20.3
	0/100	9.8	79.7	61.9	5.5
190	100/0	40.8	50.4	4.6	18.1
	0/100	7.5	76.6	61.4	2.5

Table 3. Summary of net power generation for the first 30 years.

Percent CO_2/N_2 injection	Total energy (brine) (kW-hr)	Total energy (CO_2+N_2) (kW-hr)	Total energy (brine+CO_2+N_2) (kW-hr)	Total sales @ 10¢/kW-hr (M$)	Net storage (CO_2) (MT)	Net storage (N_2) (MT)	$/MT ($CO_2$)	Average power (MWe)	Annual power sales (M$)
100/0	1.09e11	6.97e9	1.16e11	11600	447.0	0	26.0	441.1	386.7
0/100	1.78e11	5.19e9	1.83e11	18305	0	355.0	NA	695.9	610.1
20/80	1.64e11	5.55e9	1.70e11	17005	89.4	284.0	190.2	646.4	566.8
50/50	1.44e11	6.08e9	1.50e11	15003	223.4	177.5	67.2	570.4	500.3

Table 4. Summary of net power generation for the first 100 years.

Percent CO_2/N_2 injection	Total energy (brine) (kW-hr)	Total energy (CO_2+N_2) (kW-hr)	Total energy (brine+CO_2+N_2) (kW-hr)	Total sales @ 10¢/kW-hr (M$)	Net storage (CO_2) (MT)	Net storage (N_2) (MT)	$/MT ($CO_2$)	Average power (MWe)	Annual power sales (M$)
100/0	2.55e11	1.31e11	3.86e11	38600	1264	0	30.6	440.3	386.0
0/100	3.32e11	3.15e10	3.64e11	36400	0	798	NA	415.2	364.0
20/80	3.17e11	5.14e10	3.68e11	34296	252.8	638.4	135.7	419.8	343.3
50/50	2.94e11	8.13e10	3.75e11	34977	632.0	399.0	55.4	427.8	349.8

Because of the high density of cold supercritical CO_2, parasitic pumping power cost is low, consuming only 8.9 percent of gross turbine power at 200°C (Table 2). Conversely, the low density of N_2 results in greater pumping power cost, consuming 77.7 percent of gross turbine power at 200°C. The greater pumping power cost is more than compensated by N_2 being a highly efficient supplemental pressure-support fluid to drive artesian flow of brine. Prior to N_2 breakthrough at 6 years, the parasitic pumping power costs are not offset by any N_2-based power generation. During this time, 3.90×10^{10} kW-hr of brine-based power is generated, while the parasitic pumping cost of injecting N_2 at a rate of 480 kg/sec is 1.56×10^9 kW-hr, which is just 4.0 percent of the net power output. This parasitic power loss is much lower than that associated with submersible pumps. A further benefit is that brine production rates driven by artesian pressure can greatly exceed the flow capacity of submersible pumps, thereby taking advantage of the large productivity inherent to long-reach horizontal wells, providing much greater leveraging of well costs. The parasitic pumping cost for CO_2

injection is less than it is for N_2. Prior to CO_2 breakthrough at 12 years, 4.15×10^{10} kW-hr of brine-based power is generated, while the parasitic pumping cost of injecting CO_2 at a rate of 480 kg/sec is 2.58×10^{8} kW-hr, which is only 0.6 percent of the net power output. Thus, from a parasitic power cost perspective, CO_2 is a highly efficient working fluid for both heat extraction and pressure support.

During the first 30 years, the N_2-injection case generates 58 percent more power than the CO_2-injection case, primarily due to N_2 being a more efficient supplemental pressure-support fluid for generating artesian brine production. Over a 100 year period, the CO_2-injection case generates slightly more power (6 percent) than the N_2-injection case, primarily due to the increasing contribution of CO_2-based power and the fact that CO_2 is a more efficient working fluid for heat extraction than N_2. At this point we should note that the idealized homogeneous model used in this study probably underrepresents the influence of heterogeneity in causing earlier breakthrough of CO_2 and N_2 at the inner ring of producers. With earlier supplemental fluid breakthrough, the supplemental fluid will play a larger role in heat extraction and power generation. In the case of CO_2 injection, a potentially profitable strategy would be to take advantage of the preferential production of CO_2 and to possibly enhance preferential flow by adding supplemental (*make-up*) CO_2. In the case of N_2 injection, a potentially profitable strategy would be to progressively choke off N_2 production at the inner producer ring, while continuing to inject enough N_2 to maintain the ring of overpressure (Figure 4a) so that brine reinjection would continue to flow "downhill" to the outer ring of producers and thereby maintain large artesian brine production rates.

Other potentially profitable production strategies could include mixtures of CO_2 and N_2. For this reason, we considered two additional supplement fluid cases: 20/80 and 50/50 CO_2/N_2 mixtures. A 20/80 CO_2/N_2 mixture was considered because it has a similar composition to that of flue gas from fossil-energy power production. Flue gas is sometimes used in enhanced oil recovery (EOR) operations. Although currently not in commercial use, there is a patent for a multi-stage, N_2-enriched combustion process for fossil-fueled power plants that can result in a flue gas with low enough concentration of oxidants to be a suitable source of N_2 and CO_2 (Fisher and Anderson, 2004). The advantage of flue gas is its cost and availability, compared to CO_2 captured from fossil-fueled power plants. The total net power generation for the 20/80 CO_2/N_2 case is similar to that of the 0/100 case (Tables 3 and 4). The total electricity power sales per MT of stored CO_2 basis is high (>\$100/MT of CO_2) and could be economically viable even given the high cost of CO_2 capture. The 50/50 CO_2/N_2 case is also similar to the 0/100 case (Tables 3 and 4). It is interesting to note that all four cases generate a similar amount of total net power over a 100 year timeframe (Table 4).

4.4 Potential for Grid-Scale Energy Storage

For conventional geothermal power generation, the parasitic power load, which is dominated by the power required for fluid recirculation, is synchronous with the gross power output. In our approach, fluid production relies on pressure augmentation, driven by the injection of a compressible fluid. With the exception of the power required for brine reinjection (which is low, compared to the power to lift brine), the timing of the parasitic power load can be shifted so that it does not coincide with peak grid power demand. This would allow net power output to be nearly equal to gross power output during peak electricity demand. Because our approach can use a readily available supplemental fluid (N_2 separated from air), it is not limited to continuous, steady injection operations. Because energy storage is achieved by shifting when the parasitic power load occurs, it is nearly 100 percent efficient, and significantly superior to other forms of grid-scale energy storage, such as compressed air energy storage (CAES) or pumped hydroelectric storage (PHES). Integrating this form of energy storage into power grids would add an additional reason why geothermal energy is a very useful renewable energy resource; in addition to providing reliable base-load power, our geothermal energy approach can mitigate a major drawback of other renewable energy sources—their inherent variability.

5. Future Work

We present promising results for an innovative approach using CO_2 and N_2 for pressure support to drive the recirculation of CO_2, N_2, and brine as working fluids, which could contribute to the next generation of geothermal energy production. We used a homogeneous model and future work should address the impact of more realistic, heterogeneous geology and how this approach might be adapted to complex reservoir settings. Heterogeneity will result in earlier CO_2 and N_2 breakthrough, increasing the relative contribution of CO_2- and N_2-based power, while decreasing the contribution of brine-based power. Heterogeneity may also reduce net CO_2 and N_2 storage, resulting in more efficient utilization of the supplemental working fluid.

To more rigorously determine the economic benefits of this approach, it will be necessary to modify the reservoir model so that it can explicitly address injecting mixtures of CO_2 and N_2, either together or in a staged manner. Because of the importance of avoiding CO_2 flashing in the wellbore, it will be useful to consider staged injection, where N_2 injection is followed by CO_2 injection. Staged N_2/CO_2 scenarios should also consider diurnal or intermittent staging wherein N_2 is injected during periods of minimum grid power demand or when there is a surplus of renewable power on the grid. It will also be important to incorporate wellbore models of multi-phase flow of CO_2, N_2, and brine. This will be important in assessing the brine-production capacity of horizontal wells, driven by artesian pressures. Wellbore model will also allow for a more rigorous assessment of the influence of the thermosiphon effect, together with that of artesian pressure, on CO_2- and N_2-production capacity of horizontal wells. Future work should also consider well patterns with multiple levels to provide better control of fluid and energy recovery.

6. Conclusions

Stratigraphic reservoirs often have higher permeability and much greater area than typical hydrothermal systems. These advantages can lead to viable geothermal development provided heat extraction is maximized on a per well basis (which reduces drilling cost), while extraction cost (dominated by parasitic power load) is minimized. Horizontal wells are an attractive option for maximizing heat extraction on a per well basis; however, their inherent productivity is likely to exceed the capacity of submersible pumps. Much of the research in applying supercritical CO_2 to geothermal power systems has focused on using CO_2 as a working fluid. This stems from the advantageous thermophysical properties of CO_2, which can reduce the parasitic costs of powering fluid recirculation and enable more direct and efficient power conversion through a turbine. In this paper, we expand upon this idea by demonstrating how CO_2 and N_2 can be utilized as pressure-support fluids to generate artesian pressures to drive brine, CO_2, and N_2 production, thereby using all fluids as working fluids. We develop a horizontal-well concept to address the following important goals:

- Conserve pressure from injection operations to maximize the fluid-production benefit.
- Minimize the loss of CO_2 and/or N_2.
- Maximize fluid production rates on a per well basis.
- Option to shift the timing of the parasitic power load to reduce cost and enable energy storage.
- Manage overpressure to reduce related risks, such as induced seismicity and CO_2 leakage.
- Better control of fluid and energy recovery for improved sweep efficiency.
- Provide supplemental working fluids that are chemically compatible with the reservoir formation.
- Provide make-up brine for reinjection and/or for cooling-plant purposes.

For a reservoir bottom depth of 5 km, we considered a four-ring horizontal-well pattern, and find:

- A hydraulic divide is created that restricts lateral migration of CO_2 or N_2, causing CO_2 or N_2 production to only occur at the inner ring, while the outer ring only produces brine.
- Artesian pressures are created that drive large brine production rates (without submersible pumps), which generate power almost immediately, and provide a significant fraction of the total power.

- After CO_2 breakthrough, CO_2-based power increases, compensating for the decrease in brine-based power generation, resulting in sustained total power that exceeds 400 MWe for 100 years.
- Due to its lower density, N_2 is highly efficient in driving large brine production rates, particularly at early time; consequently, early time power generation is greater for N_2 injection, while late time power generation is slightly greater for CO_2 injection.
- The thermosiphon effect efficiently drives fluid recirculation; for CO_2 injection, the parasitic pumping cost is only 0.6 percent of net power output; for N_2 injection, it is 4.0 percent of net power.
- Net storage of CO_2 frees up an equivalent volume of make-up brine for reinjection, with the distinct advantage of being derived from the same formation, which reduces the possibility of chemical incompatibility.

The results of our study indicate that the multi-ring, horizontal-well approach, which uses CO_2 and/or N_2 as both pressure-support and working fluids, has the potential to improve the economic viability of geothermal energy production and provide low-cost, efficient, grid-scale energy storage in sedimentary formations.

Acknowledgements

This work was sponsored by the USDOE Geothermal Technologies Program, managed by Joshua Mengers and by Ormat Technologies, under the direction of Ezra Zemach. This work was performed under the auspices of the USDOE by LLNL under contract DE-AC52-07NA27344.

References

Adams, B., T.H. Kuehn, J.M. Bielicki, J.B. Randolph, and M.O. Saar, 2013. The importance of the thermosiphon effect in CO_2-Plume Geothermal (CPG) systems, *Applied Energy Journal*, in preparation.

ASME, 2006. ASME Steam Tables Compact Edition, ASME, Three Park Avenue, New York, NY, USA.

Brown, D.W., 2000. A hot dry rock geothermal energy concept using supercritical CO_2 instead of water, *Proceedings of the 25th Workshop on Geothermal Reservoir Engineering*, Stanford University, 233–238.

Buscheck, T.A., Y. Sun, M. Chen, Y. Hao, T.J. Wolery, W.L. Bourcier, B. Court, M.A. Celia, S.J. Friedmann, and R.D. Aines, 2012a. Active CO_2 reservoir management for carbon storage: Analysis of operational strategies to relive pressure buildup and improve injectivity, *International Journal of Greenhouse Gas Control*, **6**, 230–245, doi:10.1.1016/j.ijggc.2011.11.007.

Buscheck, T.A., T.R. Elliot, M.A. Celia, M. Chen, Y. Hao, C. Lu, and Y. Sun, 2012b. Integrated, geothermal-CO_2 storage reservoirs: adaptable, multi-stage, sustainable, energy-recovery strategies that reduce carbon intensity and environmental risk, *Proceedings for the Geothermal Resources Council 36th Annual Meeting*, 30 Sept–3 Oct, 2012, Reno, NV, USA.

Buscheck, T.A., T.R. Elliot, M.A. Celia, M. Chen, Y. Sun, Y. Hao, C. Lu, T.J. Wolery, and R.D. Aines, 2012c. Integrated geothermal-CO_2 reservoir systems: Reducing carbon intensity through sustainable energy production and secure CO_2 storage, *Proceedings of the International Conference on Greenhouse Gas Technologies (GHGT-11)*, Kyoto, Japan, 18–22 Nov, 2012.

Buscheck, T.A., M. Chen, C. Lu, Y. Sun, Y. Hao, M.A. Celia, T.R. Elliot, H. Choi, and J.M. Bielicki, 2013. Analysis of operational strategies for utilizing CO_2 for geothermal energy production, Proceedings of the 38th Workshop on Geothermal Reservoir Engineering, Stanford University, Palo Alto, CA, USA, 11–13 February, 2013.

Carr, T.R., P.M. Rich, and J.D. Bartley. 2007. The NATCARB geoportal: linking distributed data from the Carbon Sequestration Regional Partnerships. *Journal of Map and Geography Libraries: Special Issue on Department of Energy (DOE) Geospatial Science Innovations*, **4**, 131–147.

DOE, 2012. GETEM–Geothermal electricity technology evaluation model, August 2012 Beta, USDOE Geothermal Technologies Program.

Elliot, T.R., T.A. Buscheck, and M.A. Celia, 2013. Active CO_2 reservoir management for sustainable geothermal energy extraction and reduced leakage, *Greenhouse Gases: Science and Technology*, **1**, 1–16; DOI: 1002/ghg.

Fenghour, A., W.A. Wakeham, and V. Vesovic, 1998. The viscosity of carbon dioxide. *Journal of Physical and Chemical Reference Data*, **27** (1), 31–44.

Fisher, L.E. and B.L. Anderson, 2004. Multi-stage combustion using nitrogen-enriched air. US Patent 6790030 B2.

Haley, K.A., T.H. Gillham, and D. Yannimaras, 2002. West Hackberry Tertiary Project: Final Report, September 3, 1993 to March 31, 1999. DOE/BC/14963-21 (OSTI ID: 792224), Amoco Production Company, Houston TX, National Energy Technology Laboratory, National Petroleum Technology Office, US DOE, Tulsa, OK.

IPPC (Intergovermental Panel on Climate Change), 2005. Special report on carbon dioxide capture and storage. Cambridge University Press, Cambridge, UK and New York, NT, USA.

Lemmon, E.W. and R.T. Jacobsen, 2004. Viscosity and thermal conductivity equations for nitrogren, oxygen, argon, and air, *International Journal of Geophysics*, **25** (1), 21–69.

Nitao, J.J., 1998. "Reference manual for the NUFT flow and transport code, version 3.0," Lawrence Livermore National Laboratory, UCRL-MA-130651-REV-1, Livermore, CA, USA.

Pruess, K., 2006. Enhanced geothermal systems (EGS) using CO_2 as working fluid–a novel approach for generating renewable energy with simultaneous sequestration of carbon, *Geothermics*, **35**, 351–367.

Randolph, J.B. and M.O. Saar, 2011a. Coupling carbon dioxide sequestration with geothermal energy capture in naturally permeable, porous geologic formations: Implications for CO_2 sequestration. *Energy Procedia*, **4**, 2206–2213.

Randolph, J.B. and M.O. Saar, 2011b. Impact of reservoir permeability on the choice of subsurface geothermal heat exchange fluid: CO_2 versus water and native brine. *Proceedings for the Geothermal Resources Council 35th Annual Meeting*: 23–26 Oct, 2011, San Diego, CA, USA.

Randolph, J.B., and M.O. Saar, 2011c. Combining geothermal energy capture with geologic carbon dioxide sequestration, *Geophysical Research Letters*, **38**, L10401, doi:10.1029/2011GL047265.

Saar, M.O., J.B. Randolph, and T.H. Kuehn, 2010. Carbon Dioxide-based geothermal energy generation systems and methods related thereto. US Patent Application 20120001429.

Socolow, R.H. and S.W. Pacala, 2006. A plan to keep carbon in check, *Scientific American*, **295** (3), 50–57.

Span, R. and W. Wagner, 1996. A new equation of state for carbon dioxide covering the fluid region from the triple-point temperature to 1100K at pressures up to 800 MPa. *Journal of Physical and Chemical Reference Data*, **25** (6), 1509–1596.

Span, R., E.W. Lemmon, R.T. Jacobsen, W. Wagner, and A. Yokozeki, 2000. A reference equation of state for the thermodynamic properties of nitrogen for temperatures from 63.151 to 1000 K and pressures to 2200 MPa, *Journal of Physical and Chemical Reference Data*, **29** (6), 136–1433.

van Genuchten, M.T., 1980. A closed form equation for predicting the hydraulic conductivity of unsaturated soils. *Soil Science Society of America Journal*, **44**, 892–898.

Zhou, Q., J.T. Birkholzer, C-F Tsang, and J.A. Rutqvist, 2008.A method for quick assessment of CO_2 storage capacity in closed and semi-closed saline formations. *International Journal of Greenhouse Gas Control*, **2**, 626–639.